Materials Chemistry and Physics 218 (2018) 140–146

Contents lists available at ScienceDirect

Materials Chemistry and Physics

journal homepage: www.elsevier.com/locate/matchemphys

Effect of solvent in preparation of SiOC bulk ceramics

Ruixin Ma[a,b], Kathy Lu[a,*], Donald Erb[a]

[a] Department of Materials Science and Engineering, Virginia Tech, Blacksburg, VA, 24061, USA
[b] Department of Environmental Engineering, North China Institute of Science and Technology, Beijing, 101601, China

HIGHLIGHTS

- SiOC microstructure is influenced by the solvent trapped in the precursors.
- Solvent influences carbon content and crystallization of SiC during pyrolysis.
- Accelerated SiC formation is more prominent at lower pyrolysis temperature.
- SiC formation decreases with solvent content at higher pyrolysis temperature.

GRAPHICAL ABSTRACT

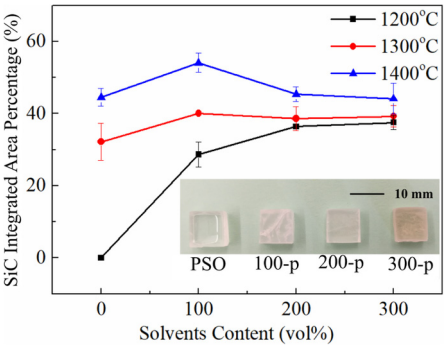

ARTICLE INFO

Keywords:
Solvent
Pentanone
Crosslinking
SiOC
Crystallization

ABSTRACT

Silicon oxycarbide (SiOC) is an important polymer derived ceramic with many unique properties such as high temperature stability and amorphous-nanocrystalline mixed structures. It can be made using different processing routes. In this study, SiOC ceramics were investigated using a polysiloxane precursor crosslinked in the presence of 0, 100, 200, and 300 vol% of 3-pentanone as the solvent. The microstructure and the phase evolution during pyrolysis depend on the solvent concentration during crosslinking. The addition of pentanone facilitates the formation of nanocrystalline SiC at pyrolysis temperatures ≤1300 °C. However, the formation of SiC decreases with increasing solvent content when pyrolyzed at 1400 °C. Simply varying the solvent concentration during crosslinking provides a unique and tunable processing route for modifying the phase formation within SiOC ceramics.

1. Introduction

Polymer derived ceramics (PDCs) have gained an increasing interest in the past decades due to a wide variety of exceptional properties such as thermal stability, electrical conductivity, and chemical and oxidation resistance [1,2]. Among various PDCs, silicon oxycarbide (SiOC) is especially important due to its amendable nano- and/or micro-structures, relatively low processing temperatures, and functional properties [3]. Due to their high temperature stability and excellent mechanical properties, SiOC ceramics are excellent candidates in applications ranging from brake pads, high temperature sensors, ceramic MEMS, and heating elements [2]. Upon pyrolysis to temperatures greater than approximately 1100 °C, the SiOC matrix contains nano-sized SiO_2 and a disordered graphitic phase [4–6]. At pyrolysis temperatures greater than 1300 °C, SiC nanocrystals form [7]. Many properties of SiOC, such as its mechanical properties, chemical durability, and electrical conductivity, depend on the phase composition within the SiOC, so controlling the phase formation is of high importance [2,8–10].

* Corresponding author. 213 Holden Hall, Virginia Tech, Blacksburg, VA, 24061, USA.
E-mail address: klu@vt.edu (K. Lu).

https://doi.org/10.1016/j.matchemphys.2018.07.043
Received 10 January 2018; Received in revised form 7 May 2018; Accepted 20 July 2018
Available online 23 July 2018
0254-0584/

Phase formation within SiOC can be greatly modified through a variety of techniques. The formation and content of SiC within SiOC, through either phase separation of the SiOC matrix or carbothermal reduction of SiO_2, has been shown to be dependent on the atomic ratios of Si, O, and C within the polymer precursors [4,5]. Further, the temperature at which phase separation and crystallization occurs can be increased by the incorporation of free carbon within the SiOC [8,11]. Solvent modification of the polymer precursor can also influence the phase formation within SiOC. After crosslinking the polymer precursor in the presence of various solvents and pyrolysis to 1300 °C, the solvent-modified polymers form more SiC than the sample with no solvent [12].

Introducing solvents into polymer precursors for SiOC fabrication has been carried out for a number of solvent-polymer systems, with the focus predominantly on the formation of porous gels [13–15]. However, the effect of solvents on other features of SiOC, such as phase formation during pyrolysis, has not been well studied. Polyhydromethylsiloxane and divinylbenzene were crosslinked in either acetone or cyclohexane and then supercritically dried using CO_2 to obtain porous aerogels. After pyrolysis at 900 °C, the gel crosslinked in acetone had a slightly smaller carbon domain size compared to the non-polar cyclohexane [13]. Polydimethylsiloxane (PDMS) and tetraethyl orthosilicate (TEOS) hybrid gels were aged in acetone, isopropanol, and n-hexane to investigate the effect of the solvents and aging time on the properties of the SiOC after pyrolysis at 1100 °C. The polar solvents, acetone and isopropanol, more easily removed the non-crosslinked PDMS molecules from the gel, affecting the carbon content after pyrolysis [14,15]. Additionally, the polar solvents decreased the carbon crystallite size as the aging time increased, while the non-polar solvent showed the opposite trend [15]. Crosslinking a polysiloxane in the presence of either 3-pentanone, n-heptane, or isobutylbenzene followed by drying and pyrolysis at 1300 °C found that increasing the solvent concentration during crosslinking led to increased SiC formation, especially for 3-pentanone [12]. However, the evolution of the phases within SiOC at different pyrolysis temperatures was not studied, which is necessary in order to fully understand the solvent's role in the modification of the phase formation within SiOC.

In this work, SiOC ceramics are fabricated by pyrolysis of a polysiloxane crosslinked in the presence of 0, 100, 200, and 300 vol% pentanone. The effects of the solvent amount on the resulting thermophysical properties, phase evolution, and microstructure of the SiOC ceramics are studied at pyrolysis temperatures from 1100 °C to 1400 °C. The samples crosslinked in the presence of pentanone have accelerated SiC formation at temperatures as low as 1200 °C, compared to 1300 °C for the sample without solvent. Further, the amount of SiC formed at lower temperatures is shown to be directly related to the pentanone concentration during crosslinking.

2. Experimental procedures

A commercial polysiloxane (PSO, $[-Si(C_6H_5)_2O-]_3[-Si(CH_3)(H)O-]_2[-Si(CH_3)(CH=CH_2)O-]_2$, SPR-684, Starfire Systems, Inc., Gelest Inc., Schenectady, NY) was chosen as the base precursor and 2.1–2.4% platinum-divinyltetramethyldisiloxane complex in xylene (Pt catalyst, Gelest Inc., Morrisville, PA) was used as the catalyst. The solvent used was 3-pentanone (Fisher Scientific, Pittsburgh, PA).

Solutions with PSO and either 0, 100, 200, or 300 vol% pentanone solvent (relative to the PSO volume) were sonicated for 10 min and then mixed in a high energy mill (SPEX 8000 M Mixer/Mill, SPEX SamplePrep, Metuchen, NJ) for 10 min to form a homogeneous mixture. Next, the Pt catalyst (1 wt% relative to PSO) was added, the mixtures were mixed again in a high energy ball mill for 5 min, and then poured into aluminum foil molds. The mixtures were placed into a vacuum chamber and vacuumed for 10 min at 200 Torr to remove any bubbles in the solutions. The molds were then sealed in acid digestion vessels to prevent evaporation of the solvents and placed in an oven to crosslink at 50 °C for 12 h and then at 120 °C for 6 h. After crosslinking, the molds were removed from the acid digestion vessels and sealed for room temperature aging for 10 days to allow for the slow evaporation of the pentanone from the crosslinked samples. Samples designated as PSO corresponded to the pure PSO sample; samples with solvent additions were labelled as X-p, and X is the volume percent of pentanone (100, 200, or 300), as shown in Fig. 1. The pure PSO green body was transparent, and the transparency decreased with the amount of pentanone. Also, cracks formed in the 100-p samples during the drying process.

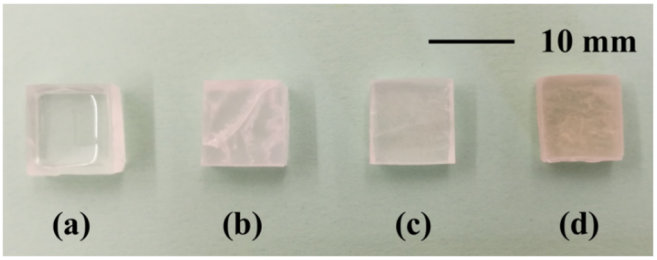

Fig. 1. Photographs of (a) pure PSO, (b) 100-p, (c) 200-p, and (d) 300-p after crosslinking and drying.

For pyrolysis, the crosslinked materials were cut and polished into square shapes roughly 10 mm in edge length and 2 mm in thickness. Next, the samples were placed into a zirconia crucible, covered on both sides with graphite mats in order to reduce friction during shrinkage and prevent warping, and put into a tube furnace (1730-20 Horizontal Tube Furnace, CM Furnaces Inc., Bloomfield, NJ). The samples were pyrolyzed in argon with a flow rate of about 500 std cm^3/min and a heating rate of 1 °C/min, held at peak temperatures between 1100°C and 1400 °C for 2 h, cooled to 400 °C with a rate of 1 °C/min, and finally cooled to 50 °C with a rate of 2 °C/min.

The chemical bonding of the polymers was evaluated using Fourier Transform Infrared Spectroscopy (FT-IR) (Nicolet 8700 with Pike GladiATR attachment, Thermo Scientific, Waltham, MA), which recorded light absorption between 500 and 4000 cm^{-1} wavenumber with a resolution of 4 cm^{-1} and averaged between 64 scans. Ceramic yield was calculated by measuring the mass of the samples before and after pyrolysis. The volume shrinkage of the samples was calculated by measuring the dimensions of regularly shaped samples before and after pyrolysis. The bulk density and porosity of the polymers and SiOC were measured using the Archimedes method with water as the saturating and submersion medium. The phase compositions of the pyrolyzed samples were analyzed in an X'Pert PRO diffractometer (PANalytical B.V., EA Almelo, the Netherlands) with Cu Kα radiation. The microstructures of the pyrolyzed ceramics were studied using a field emission SEM (LEO 1550, Carl Zeiss MicroImaging, Inc, Thornwood, NY).

3. Results and discussion

3.1. Solvent effects during crosslinking

A solvent can play an important role in the polymer crosslinking process, especially for a closed system. In this study, the crosslinking happens at 120 °C while the boiling point of 3-pentanone is 102 °C, so it is necessary to know how much solvent remains in the liquid phase mixed with the PSO. Assuming that all the 3-pentanone is kept in the sealed vessel, the evaporated solvent amount can be approximately calculated. First, the vapor pressure of the pentanone can be calculated using the Antoine equation, a simplified Clausius-Clapeyron equation [16]:

$$\log P = A - B/(T + C) \quad (1)$$

where P is the vapor pressure (Pa), T is the temperature (K), and A, B, and C are constants. For 3-pentanone, the values for A, B, and C are 9.15,1309.65, and −59.03, respectively [17]. Therefore, the vapor pressure of the pentanone at 120 °C is 169600 Pa. The amount of the

Table 1
Theoretically calculated solvent remaining in the crosslinked samples.

Sample	100-p	200-p	300-p
Original solvent content/vol%	100	200	300
Value of V in equation 2/mm^3	88944.5	84174.5	79404.5
Calculated gas amount/mol	0.00462	0.00437	0.00412
Solvent content after crosslinking/vol%	89.77	188.45	288.01

solvent in the gas phase can then be calculated by the ideal gas equation:

$$PV = nRT \quad (2)$$

where P is the vapor pressure from Equation (1) (Pa), V is the volume of the sealed container minus the initial PSO and pentanone volumes (m^3), n is the amount of the gas (mol), R is the ideal gas constant (8.314 J/mol·K), and T is the absolute temperature of the gas (K). The amount of gaseous pentanone in the sealed container can be obtained by Equation (2), and thus the amount of the solvent left in the crosslinked samples can be calculated, and the results are shown in Table 1. As shown in Table 1, the actual solvent volume within the mixture at 120 °C relative to the PSO volume is 89.77%, 188.45%, and 288.01% for the 100-p, 200-p, and 300-p samples, respectively. Although some solvent evaporates into the vapor phase during the crosslinking, most of the solvent is kept in the mixtures, so the decrease of the solvent amount is negligible for all of the samples.

The amount of pentanone remaining within the solvent-containing samples after aging, calculated by comparing the masses before and after aging, are 21.98 ± 3.59 wt%, 29.40 ± 3.07 wt%, and 30.99 ± 3.67 wt% for the 100-p, 200-p, and 300-p samples, respectively. However, it is unclear whether pentanone is trapped between the polymer chains or crosslinked with the polymer molecules. To answer this question, the TGA data of the crosslinked samples are shown in Fig. 2. There is no mass loss when the temperature is lower than 300 °C for the pure PSO. However, there is about 10% mass loss for the pentanone-containing samples between 100°C and 300 °C. This must be due to the evaporation of the solvent because the boiling point of 3-penanone is 102 °C. It also confirms that pentanone is trapped in the polymer and not crosslinked with the polymer. Fig. 2 further shows that the mass loss of the pentanone-containing samples is about 10% at 300 °C, lower than the total solvent content remaining in the aged green body. Therefore, there should still be some solvent trapped within the samples after the free pentanone evaporation. It is also worth noting that the 100-p sample shows the largest mass loss between 400°C and 600 °C; this phenomenon will be explained later.

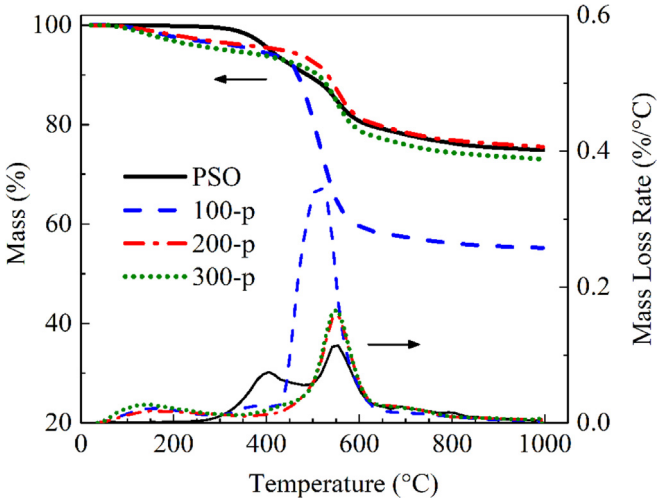

Fig. 2. TGA and dTG results of the pure PSO and solvent-containing samples.

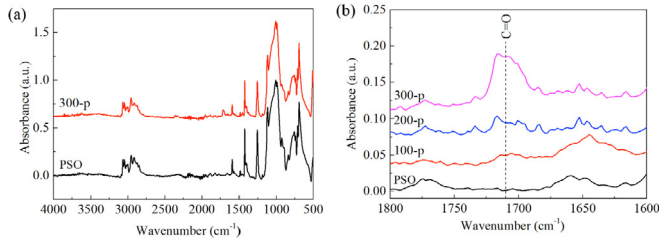

Fig. 3. FT-IR spectra of the pure PSO and pentanone-containing samples after crosslinking.

Fig. 3 shows the FT-IR spectra of the crosslinked PSO with and without pentanone. Both the pure PSO and 300-p samples (FT-IR curves for the other samples are omitted for brevity) show sharp peaks at approximately 695, 715, 740, 1130, 1426, and between 3000 and 3100 cm^{-1} wavenumber (Fig. 3(a)), which are characteristic of the phenyl side group in the base PSO. A peak at 1260 cm^{-1} wavenumber corresponds to the methyl side group, a broad peak between 1000 and 1100 cm^{-1} wavenumber can be assigned to Si-O-Si, and the peaks between 2868 and 2960 cm^{-1} correspond to CH_x bonds [18,19]. The solvent presence during crosslinking does not affect the chemical bonding or crosslinking behavior of the PSO polymer. In Fig. 3(b), however, as the pentanone content increases, a peak at 1710-1720 cm^{-1} wavenumber becomes more obvious, which is characteristic of the carbonyl functional group [20]. Since there is no carbonyl group in the base PSO, it must come from the 3-pentanone solvent. This means that some pentanone is trapped in the PSO polymer during the crosslinking as already discussed.

3.2. Shrinkage and ceramic yield

All the samples are intact and show good shape retention after the pyrolysis. The volume shrinkage and ceramic yield for the samples after pyrolysis are shown in Table 2. The volume shrinkages for all of the samples are in the range of 24.25%–53.52%. At the same pyrolysis temperature, as the solvent content increases, the volume shrinkage slightly decreases (except for the 100-p samples). This is mainly because of the pores created by the solvent evaporation and decomposition during the pyrolysis. As a result, higher solvent content leads to less shrinkage (except for the 100-p samples). However, the volume shrinkages of the 100-p samples are much lower. This is because these samples expand in the thickness direction and shrink in the lateral direction. All the other samples shrink in all directions.

There are two reasons for the thickness expansion of the 100-p samples. The first is likely due to the uneven distribution of the solvent. During the crosslinking process, the pentanone volume percent is 89.77% in the 100-p sample; the PSO chains are coiled and not mixed evenly with pentanone. During aging, the unevenly distributed solvent evaporates non-uniformly and leads to pores and/or cracks. The other reason could be insufficient crosslinking. The mixture of the solvent and polymer is probably a two-phase system. So, the PSO crosslinks more thoroughly in some regions but not in others. Cracks, pores, and non-uniform crosslinking can cause the samples to expand in the smaller dimension direction.

The ceramic yields for the samples are 48.18%–72.43%. At the same solvent content, the ceramic yield decreases with the temperature increase. This could be understood as follows: during the pyrolysis of the preceramic at 1100°C-1400 °C, the following reactions take place [21–23]:

$$2SiOC \rightarrow SiO_2(amorphous) + SiC(\beta) + C(graphite) \quad (3)$$

$$SiO_2(amorphous) + 3C(graphite) \rightarrow SiC(\beta) + 2CO\uparrow \quad (4)$$

Equation (3) represents the SiOC phase separation into amorphous SiO_2, SiC(β), and free carbon, and Equation (4) indicates that

Table 2
Shrinkage and ceramic yield of the pure PSO and pentanone-containing samples.

Sample	Volume shrinkage (%)				Ceramic Yield (%)			
	1100 °C	1200 °C	1300 °C	1400 °C	1100 °C	1200 °C	1300 °C	1400 °C
PSO	53.46 ± 2.23	50.76 ± 1.32	52.76 ± 0.80	53.52 ± 1.71	69.35 ± 0.12	70.43 ± 0.47	68.43 ± 0.17	67.04 ± 0.90
100-p	25.31 ± 1.24	27.36 ± 3.08	24.25 ± 1.33	28.20 ± 2.32	52.46 ± 0.64	55.71 ± 1.14	49.94 ± 2.41	48.18 ± 1.38
200-p	45.55 ± 0.12	48.57 ± 0.84	46.79 ± 1.66	48.10 ± 1.55	72.43 ± 0.29	71.62 ± 1.20	71.63 ± 0.75	67.18 ± 2.28
300-p	32.60 ± 0.12	46.07 ± 1.50	43.51 ± 3.29	47.30 ± 2.26	64.03 ± 0.64	70.67 ± 0.46	63.16 ± 0.17	65.54 ± 0.96

carbothermal reaction occurs between SiO_2 and free carbon, producing SiC(β) and CO gas. For the base PSO, higher pyrolysis temperatures lead to more SiC formation and CO release [23]. At the same pyrolysis temperature, an increase in the pentanone content results in a decrease in the ceramic yield (except for the 100-p samples). This is understandable in light of the carbon-enhancing effect from pentanone. More pentanone content leads to more free carbon during pyrolysis, and more carbon formation in general leads to a lower ceramic yield [8].

The ceramic yield for the 100-p samples is consistent with the TGA data shown in Fig. 2. It also indicates that there are uncrosslinked polymer chains in the 100-p sample. These uncrosslinked chains decompose and give off gaseous species, which in turn leads to the lower ceramic yield.

Additionally, the pure PSO samples have the highest yield. This is because PSO is a single-phase system and the polymer chains are more likely to crosslink and convert into ceramics. The 100-p samples contain unevenly dispersed pentanone, so the mixture is likely a two-phase system and has lower thermal stability during pyrolysis. For the 200-p and 300-p samples, the PSO molecules can fully expand in the solvent and the phase conversion is not compromised.

The bulk density of the SiOC samples after pyrolysis ranges from 1.05 g/cm^3 to 1.84 g/cm^3 as shown in Table 3. The 100-p samples show significant bulk density differences from the other samples, with much lower bulk densities and higher open porosities. This is mainly because of the solvent's influence during the crosslinking and aging. Since the solvent volume is the same as the PSO volume in the 100-p sample, it is difficult to mix them thoroughly. Therefore, pentanone molecules are trapped but not uniformly distributed. The resulting defects cause uneven expansion in the thickness direction during the pyrolysis and thus lower bulk density.

The generally lower porosity for the 200-p and 300-p samples can be understood as follows: pentanone and PSO mix uniformly, but the molecular volume of pentanone is 0.18 nm^3. Thus, it could create tiny pores during crosslinking. During aging, these pores experience a capillary pressure P, depending on the solvent surface tension γ, pore radius r, and contact angle θ [24]:

$$P = 2\gamma\frac{cos(\theta)}{r} \quad (5)$$

The surface tension of pentanone is 24.7 mN/m [25], so the pore radius should be 0.35 nm if a spherical pore shape is assumed. Therefore, the high surface tension and small pore radius would cause a high capillary pressure during drying, making the pores more likely to collapse and leading to low porosity after pyrolysis.

The pentanone molecules trapped in the green body after aging could decompose during pyrolysis and produce CO, CH_3, and C_2H_4 [26]. Two CH_3 radicals can react to form methane, ethylene, and hydrogen [27].

$$CH_3CH_2COCH_2CH_3 \rightarrow CO\uparrow + 2CH_3 + C_2H_4\uparrow \quad (6)$$

$$2CH_3 \rightarrow CH_4\uparrow + C_2H_4\uparrow + H_2\uparrow \quad (7)$$

Therefore, the decomposition of pentanone during pyrolysis can create pores in the samples. The porosity of the 300-p sample is higher because of the higher solvent content in the samples.

3.3. Phase evolution

As shown in Fig. 4(a), all the XRD patterns have an amorphous SiO_2 halo at ~22° [28], and a broad peak at ~43°, the latter can be assigned to disordered carbon of a turbostractic structure [28–31]. According to the height of the peak, the amount of C_{free} is generally proportional to the solvent content at 1100 °C. This can be explained based on the decomposition of the solvent.

Comparing Fig. 4(a) and (b), for the pure PSO samples, the XRD patterns at 1100 °C and 1200 °C both show an amorphous structure with only the presence of the SiO_2 halo and carbon diffraction peak, which means that the phase separation is yet to happen. This is consistent with the earlier report that the phase separation of PSO occurs at 1200–1300 °C [32,33]. However, for the solvent-containing samples, with the pyrolysis temperature increase to 1200 °C, diffraction peaks at 35.5°, 60°, and 72° appear, corresponding to the (111), (220), and (311) crystallographic planes of β-SiC [19]. This means that the phase separation in the solvent-containing samples takes place between 1100°C and 1200 °C, which is obviously earlier than that of the pure PSO sample. Furthermore, the amount of β-SiC in the solvent-containing samples is proportional to the solvent content, proving that the SiC crystallization is influenced by the solvent amount and thus carbon content. Carbon content accelerates the onset of the SiC crystallization [34]. Increasing the pyrolysis temperature further results in more intense β-SiC peaks, consistent with previous studies of SiOC systems [35–37].

To better understand the β-SiC formation, all of the XRD peaks (23°, 35.6°, 43°, 60°, and 72°) were fitted using Pearson VII distributions, and the percentages of the integrated area of the SiC peaks (35.6°, 60°, 72°) compared to the total peak area for each sample at different pyrolysis temperatures are shown in Fig. 5. According to Fig. 5, at a pyrolysis temperature of 1200 °C, the SiC content is proportional to the solvent content. At 1300 °C, the SiC contents of the solvent-containing samples

Table 3
Bulk density and open porosity of the PSO and pentanone-containing samples.

Sample	Bulk density (g/cm^3)				Open porosity (%)			
	1100 °C	1200 °C	1300 °C	1400 °C	1100 °C	1200 °C	1300 °C	1400 °C
PSO	1.80 ± 0.01	1.84 ± 0.02	1.75 ± 0.04	1.70 ± 0.03	5.11 ± 0.56	5.05 ± 0.34	8.77 ± 1.70	9.60 ± 0.76
100-p	1.05 ± 0.03	1.09 ± 0.05	1.05 ± 0.07	1.07 ± 0.05	24.72 ± 4.16	31.37 ± 1.46	31.69 ± 4.11	30.72 ± 2.20
200-p	1.74 ± 0.01	1.76 ± 0.01	1.78 ± 0.01	1.66 ± 0.05	0.92 ± 0.27	1.00 ± 0.19	4.90 ± 0.74	6.47 ± 1.17
300-p	1.60 ± 0.03	1.70 ± 0.01	1.58 ± 0.02	1.67 ± 0.02	7.98 ± 1.51	4.95 ± 0.29	9.95 ± 0.13	6.00 ± 0.98

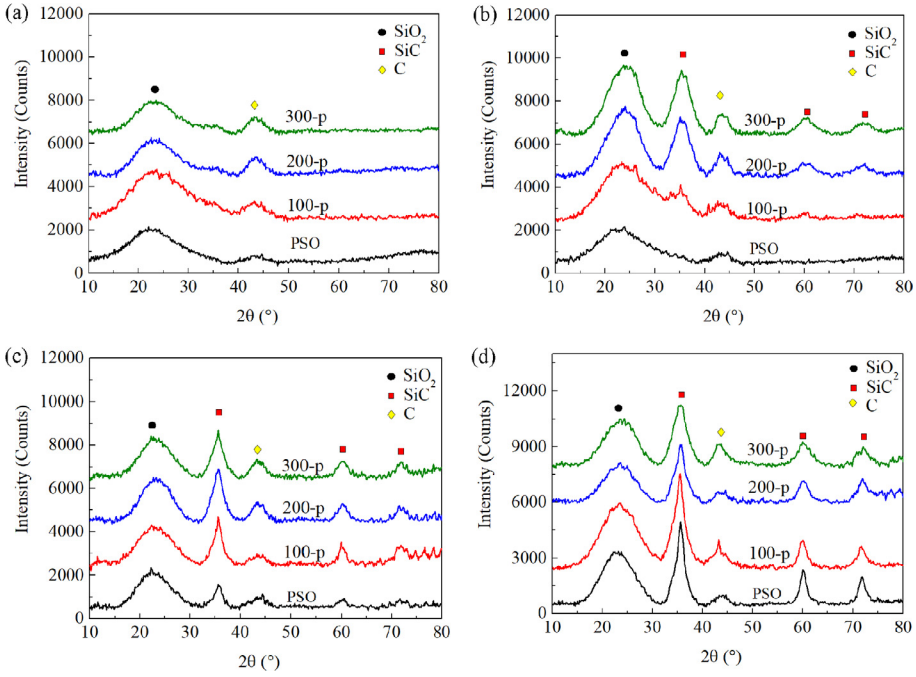

Fig. 4. XRD patterns for different solvent amount samples after pyrolysis at (a) 1100 °C, (b) 1200 °C, (c) 1300 °C, and (d) 1400 °C.

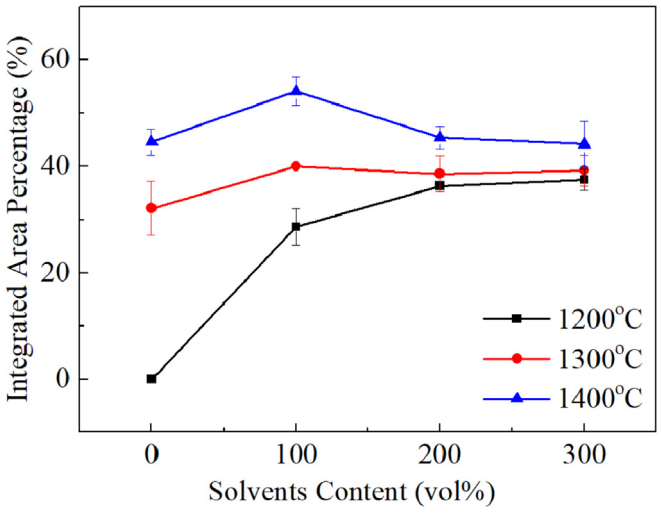

Fig. 5. XRD area percent of SiC for the pyrolyzed samples.

are almost the same but all higher than that of the pure PSO. At 1400 °C pyrolysis temperature, the SiC content is the highest for the 100-p sample while the other three samples have almost the same SiC content.

The different trends in the SiC formation can be explained as follows. The pure PSO sample is composed of a Si-O-C glassy matrix with free carbon homogenously dispersed and embedded inside the matrix [38]. With the temperature increase, the SiOC phase separates into a more stable SiO_2 glassy matrix, amorphous SiC, and highly disordered graphite-like carbon [5,38]. The amorphous SiOC may crystallize by two routes [5]: phase separation (Equation (3)) and carbothermal reduction (Equation (4)). The phase separation leads to no mass loss, but the carbothermal reaction causes more mass loss because of the fugitive CO gas.

At a pyrolysis temperature of 1200 °C, the 300-p sample has the most SiC content. However, there is no obvious difference in the ceramic yield between the PSO and 300-p samples (shown in Table 2). Therefore, carbothermal reduction is not the pathway for the β-SiC formation. The carbon produced by the solvent decomposition facilitates and accelerates the β-SiC formation. When the temperature is 1300 °C, most β-SiC results from the phase separation but the extra carbon is still involved in the SiC formation, so the solvent-containing samples show more SiC than the pure PSO sample (Fig. 5). The SiC percent trend is reversed when the temperature reaches 1400 °C. This is because the presence of turbostratic carbon can act as a physical barrier between the SiC nuclei and the amorphous SiOC phase to hinder further phase separation of the SiOC [7,8,23,37].

Among the solvent-containing samples, the 100-p sample always shows the most β–SiC content increase between each temperature interval. This is mainly because the 100-p sample has the highest open porosity. SiC nanowires have been observed in the pores, consistent with previous studies showing that nanowires form via a gas-gas reaction when adequate reactant gases are supplied [39–41]; this is a likely explanation of the significant nanocrystalline SiC formation in the 100-p sample at 1400 °C [42]. The porous structure can provide enough space for gas diffusion and SiC nanorod formation [43–46]. In this work, the SiO gas could be created according to Equation (9) because of the carbon provided by pentanone decomposition. β-SiC can be obtained from the pentanone decomposition following Equation (10).

$$SiO_2(s) + C(s) \rightarrow SiO(g) + CO(g) \quad (9)$$

$$SiO(g) + 3CO(g) \rightarrow \beta\text{-}SiC(s) + 2CO_2(s) \quad (10)$$

To further understand the phase separation, the microstructures of the PSO and 200-p samples pyrolyzed at 1200 °C and 1400 °C are shown in Fig. 6. The samples pyrolyzed at 1400 °C shows more texture than those at 1200 °C. At the same temperature of 1200 °C, the 200-p sample shows more texture. Even though the texture is not a direct indication of crystallite sizes, this could signify that the phase separation is more aggressive at higher temperatures and at higher solvent contents. These are consistent with the results in Fig. 4.

4. Conclusions

A polysiloxane crosslinked with different pentanone concentrations has been investigated in order to understand the influence of the solvent on the microstructural evolution of the resulting bulk SiOC ceramics. The pentanone added before crosslinking can be trapped in the

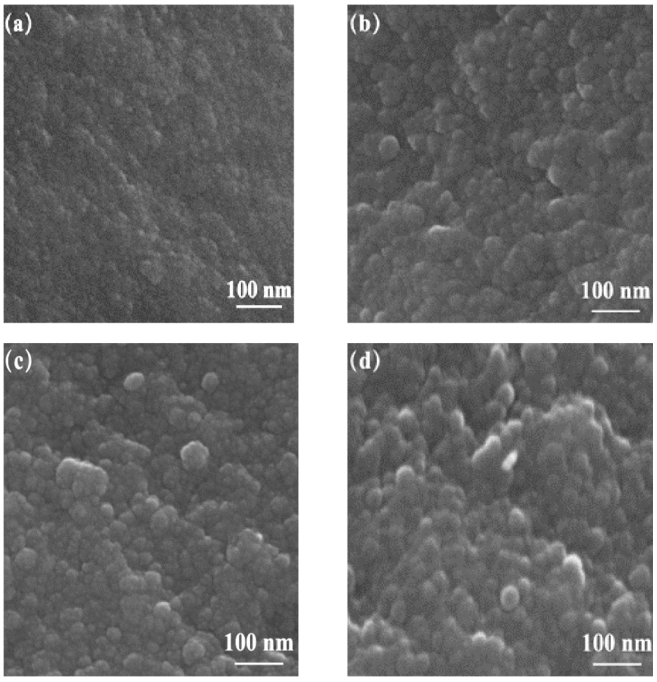

Fig. 6. SEM fracture surface of (a) PSO pyrolyzed at 1200 °C; (b) PSO pyrolyzed at 1400 °C; (c) 200-p pyrolyzed at 1200 °C; (d) 200-p pyrolyzed at 1400 °C.

green body after drying and subsequently impact the pyrolysis behavior of the polymer. For the samples crosslinked with a low amount of pentanone, the pyrolyzed SiOC experiences more mass loss during pyrolysis and has a drastically increased open porosity of 24.72%–31.69%. At pentanone concentrations of ≥200 vol%, the ceramic yield, linear shrinkage, and open porosity values more closely resemble those of the sample without any solvent, but the solvent samples form SiC at pyrolysis temperatures lower than for the sample crosslinked without pentanone. The preferential SiC formation is shown to be directly dependent on the pentanone concentration and is attributed to pentanone and its decomposition products, which increase the carbon content within the SiOC ceramics. The accelerated SiC formation caused by the solvent is more prominent at lower pyrolysis temperatures (≤1300 °C). At a higher pyrolysis temperature of 1400 °C, SiC formation decreases with increasing solvent content. The ability to adjust the SiC content and formation temperature within SiOC ceramics by simply controlling the solvent concentration during crosslinking is a novel and simple approach that can be used in applications requiring bulk SiOC.

Conflicts of interest

The authors declare that they have no conflict of interest.

Acknowledgements

We acknowledge the financial support from National Science Foundation under grant number CMMI-1634325.

References

[1] E. Ionescu, H.J. Kleebe, R. Riedel, Silicon-containing polymer-derived ceramic nanocomposites (PDC-NCS): preparative approaches and properties, Chem. Soc. Rev. 41 (2012) 5032–5052.
[2] P. Colombo, G. Mera, R. Riedel, G.D. Soraru, Polymer-derived ceramics: 40 years of research and innovation in advanced ceramics, J. Am. Ceram. Soc. 93 (2010) 1805–1837.
[3] K. Lu, Porous and high surface area silicon oxycarbide-based materials-a review, Math. Sci. Eng. R 97 (2015) 23–49.
[4] H. Brequel, J. Parmentier, G.D. Soraru, L. Schiffini, S. Enzo, Study of the phase separation in amorphous silicon oxycarbide glasses under heat treatment, Nanostruct. Mater. 11 (1999) 721–731.
[5] A. Saha, R. Raj, Crystallization maps for SiCO amorphous ceramics, J. Am. Ceram. Soc. 90 (2007) 578–583.
[6] A. Saha, R. Raj, D.L. Williamson, A model for the nanodomains in polymer-derived SiCO, J. Am. Ceram. Soc. 89 (2006) 2188–2195.
[7] H. Brequel, J. Parmentier, S. Walter, R. Badheka, G. Trimmel, S. Masse, J. Latournerie, P. Dempsey, C. Turquat, A. Desmartin-Chomel, L. Le Neindre-Prum, U.A. Jayasooriya, D. Hourlier, H.J. Kleebe, G.D. Soraru, S. Enzo, F. Babonneau, Systematic structural characterization of the high-temperature behavior of nearly stoichiometric silicon oxycarbide glasses, Chem. Mater. 16 (2004) 2585–2598.
[8] J. Zhao, R. Xu, G.X. Luo, J. Wu, H.S. Xia, Self-healing poly(siloxane-urethane) elastomers with remoldability, shape memory and biocompatibility, Polym. Chem. 7 (2016) 7278–7286.
[9] G.D. Soraru, E. Dallapiccola, G. DAndrea, Mechanical characterization of sol-gel-derived silicon oxycarbide glasses, J. Am. Ceram. Soc. 79 (1996) 2074–2080.
[10] G.D. Soraru, S. Modena, E. Guadagnino, P. Colombo, J. Egan, C. Pantano, Chemical durability of silicon oxycarbide glasses, J. Am. Ceram. Soc. 85 (2002) 1529–1536.
[11] Y.D. Blum, D.B. MacQueen, H.-J. Kleebe, Synthesis and characterization of carbon-enriched silicon oxycarbides, J. Eur. Ceram. Soc. 25 (2005) 143–149.
[12] D. Erb, K. Lu, Synthesis of SiOC using solvent-modified polymer precursors, Mater. Chem. Phys (2018) Submitted.
[13] P.V.W. Sasikumar, E. Zera, M. Graczyk-Zajac, R. Riedel, G.D. Soraru, Structural design of polymer-derived SiOC ceramic aerogels for high-rate Li ion storage applications, J. Am. Ceram. Soc. 99 (2016) 2977–2983.
[14] A. Tamayo, J. Rubio, Structure modification by solvent addition into TEOS/PDMS hybrid materials, J. Non-Cryst. Solids 356 (2010) 1742–1748.
[15] A. Tamayo, J. Rubio, F. Rubio, J.L. Oteo, R. Riedel, Texture and micro-nanostructure of porous silicon oxycarbide glasses prepared from hybrid materials aged in different solvents, J. Eur. Ceram. Soc. 31 (2011) 1791–1801.
[16] G.W. Thomson, The antonie equation for vapor-pressure data, Chem. Rev. 38 (1) (1946) 1–39.
[17] R.R.C. Collerson, J.F, R. Handley, J.F. Martin, C.H.S. Sprake, Thermodynamic properties of organic oxygen compounds. Part xv. Purification and vapour pressures of some ketones and ethers, J. Chem. Soc. (Lond.) (1965) 3697–3700.
[18] G.W. Liu, J. Kaspar, L.M. Reinold, M. Graczyk-Zajac, R. Riedel, Electrochemical performance of DVB-modified SiOC and SiCN polymer-derived negative electrodes for lithium-ion batteries, Electrochim. Acta 106 (2013) 101–108.
[19] D. Erb, K. Lu, Additive and pyrolysis atmosphere effects on polysiloxane-derived porous SiOC ceramics, J. Eur. Ceram. Soc. 37 (2017) 4547–4557.
[20] N. Fuson, M.L. Josien, E.M. Shelton, An infrared spectroscopic study of the carbonyl stretching frequency in some groups of ketones and quinones, J. Am. Chem. Soc. 76 (1954) 2526–2533.
[21] S. Yu, R. Tub, T. Goto, Preparation of SiOC nanocomposite films by laser chemical vapor deposition, J. Eur. Ceram. Soc. 36 (2016) 403–409.
[22] T.H. Xu, Q.S. Ma, Z.H. Chen, Mechanical property and microstructure evolutions of C_f/SiOC composites with increasing annealing temperature in reduced pressure environment, Ceram. Int. 38 (2012) 605–611.
[23] J.K. Li, K. Lu, T.S. Lin, F.Y. Shen, Preparation of micro-/mesoporous SiOC bulk ceramics, J. Am. Ceram. Soc. 98 (2015) 1753–1761.
[24] S. Smitha, P. Shajesh, P.R. Aravind, S.R. Kumar, P.K. Pillai, K.G.K. Warrier, Effect of aging time and concentration of aging solution on the porosity characteristics of subcritically dried silica aerogels, Microporous Mesoporous Mater. 91 (2006) 286–292.
[25] J.R. Rumble, CRC Handbook of Chemistry and Physics, 98th ed., CRC Press/Taylor & Francis, Boca Raton, FL, 2005.
[26] E.E. Dames, K.Y. Lam, D.F. Davidson, R.K. Hanson, An improved kinetic mechanism for 3-pentanone pyrolysis and oxidation developed using multispecies time histories in shock-tubes, Combust. Flame 161 (2014) 1135–1145.
[27] F.O. Rice, R.E. Vollrath, The thermal decomposition of acetone in the gaseous state, Proc. Natl. Acad. Sci. U. S. A 15 (1929) 702–705.
[28] R. Peña-Alonso, G.D. Sorarù, R. Raj, Preparation of ultrathin-walled carbon-based nanoporous structures by etching pseudo-amorphous silicon oxycarbide ceramics, J. Am. Ceram. Soc. 89 (2006) 2473–2480.
[29] A.M. Wilson, G. Zank, K. Eguchi, W. Xing, B. Yates, J.R. Dahn, Pore creation in silicon oxycarbides by rinsing in dilute hydrofluoric acid, Chem. Mater. 9 (1997) 2139–2144.
[30] R. Pena-Alonso, G. Mariotto, C. Gervais, F. Babonneau, G.D. Soraru, New insights on the high-temperature nanostructure evolution of SiOC and B-doped siboc polymer-derived glasses, Chem. Mater. 19 (2007) 5694–5702.
[31] Z.Q. Li, C.J. Lu, Z.P. Xia, Y. Zhou, Z. Luo, X-ray diffraction patterns of graphite and turbostratic carbon, Carbon 45 (2007) 1686–1695.
[32] J.K. Li, K. Lu, Highly porous sioc bulk ceramics with water vapor assisted pyrolysis, J. Am. Ceram. Soc. 98 (2015) 2357–2365.
[33] X. Yan, D. Su, S.S. Han, Phase separation induced macroporous SiOC ceramics derived from polysiloxane, J. Eur. Ceram. Soc. 35 (2015) 443–450.
[34] K. Lu, J.K. Li, Fundamental understanding of water vapor effect on SiOC evolution during pyrolysis, J. Eur. Ceram. Soc. 36 (2016) 411–422.
[35] H.J. Kleebe, C. Turquat, G.D. Soraru, Phase separation in an SiCO class studied by transmission electron microscopy and electron energy-loss spectroscopy, J. Am. Ceram. Soc. 84 (2001) 1073–1080.
[36] E. Ionescu, B. Papendorf, H.J. Kleebe, F. Poli, K. Muller, R. Riedel, Polymer-derived silicon oxycarbide/hafnia ceramic nanocomposites. Part i: phase and microstructure evolution during the ceramization process, J. Am. Ceram. Soc. 93 (2010) 1774–1782.
[37] Y.D. Blum, D.B. MacQueen, H.J. Kleebe, Synthesis and characterization of carbon-

enriched silicon oxycarbides, J. Eur. Ceram. Soc. 25 (2005) 143–149.
[38] M. Alejandra Mazoa, Aitana Tamayoa, Amador C. Caballerob, Juan Rubio, Electrical and thermal response of silicon oxycarbide materialsobtained by spark plasma sintering, J. Eur. Ceram. Soc. 37 (2017) (2017) 2011–2020.
[39] C.W. Pinion, J.D. Christesen, J.F. Cahoon, Understanding the vapor-liquid-solid mechanism of si nanowire growth and doping to synthetically encode precise nanoscale morphology, J. Mater. Chem. C 4 (2016) 3890–3897.
[40] J.M. Pan, X. Cheng, In situ synthesis and electriacal properties of porous SiOC ceramics decorated with SiC nanowires, Ceram. Int. 42 (2016) 12345–12351.
[41] R.S. Wagner, W.C. Ellis, Vapor-liquid-solid mechanism of crystal growth, JOM (J. Occup. Med.) 4 (1964) 89–90.
[42] Y. Wu, P. Yang, Germanium nanowire growth via simple vapor transport, Chem. Mater. 12 (2000) 605–607.
[43] C. Liu, X.Y. Meng, X.H. Zhang, C.Q. Hong, J.C. Han, W.B. Han, B.S. Xu, S. Dong, S.Y. Du, High temperature structure evolution of macroporous SiOC ceramics prepared by a sol-gel method, Ceram. Int. 41 (2015) 11091–11096.
[44] J.M. Pan, X.N. Cheng, X.H. Yan, J.F. Pan, C.H. Zhang, Q.B. Lu, Synthesis and growth of SiC/SiO_2 nanocables decorated with laminated porous ceramics from filter paper and polymeric precursor, Ceram. Int. 39 (2013) 6131–6137.
[45] J.M. Pan, X.N. Cheng, X.H. Yan, C.H. Zhang, G.F. Xu, In situ synthesis and growth mechanism of SiC nanowires in SiCO porous ceramics, J. Inorg. Mater. 28 (2013) 474–478.
[46] X.H. Zhang, J.X. Gao, C.Q. Hong, J.C. Han, W.B. Han, Observation of SiC nanodots and nanowires in situ growth in SiOC ceramics, CrystEngComm 15 (2013) 7803–7807.